Complexity of the hot carrier relaxation in Si nanowires compared to bulk

Jing Li,[1,*] Yann-Michel Niquet,[2,†] and Christophe Delerue[3,‡]
[1]*Université Grenoble Alpes, CNRS, Institut Néel, F-38042 Grenoble, France*
[2]*CEA, INAC-MEM, L_Sim, F-38000 Grenoble, France and Université Grenoble Alpes, INAC-MEM, L_Sim, F-38000 Grenoble, France*
[3]*Université Lille, CNRS, Centrale Lille, ISEN, Université Valenciennes, UMR 8520 - IEMN, F-59000 Lille, France*
(Received 25 January 2017; revised manuscript received 5 April 2017; published 1 May 2017)

We investigate the relaxation of hot carriers by emission of phonons in bulk Si and Si nanowires (NWs) with an identical atomistic methodology. The phonon scattering is strongly enhanced in NWs. At high excitation energy, the carrier cooling is faster in NWs than in bulk, mainly due to the coupling to surface phonons. Slow relaxation is only noticed for electrons at low energy in the conduction band of thin NWs due to the quantum confinement that lifts the degeneracy of the valleys. This work gives insight into the complexity of the carrier cooling in semiconductor nanostructures.

DOI: 10.1103/PhysRevB.95.205401

I. INTRODUCTION

The relaxation of hot carriers by emission of phonons (carrier cooling) is a physical process of high importance in many semiconductor devices [1]. It is one of the main sources of loss in photovoltaic materials [2] and it generates hot spots in the drain region of nanoscale transistors [3]. Hot carriers are involved in the efficiency droop of light-emitting devices [4] and in the degradation of field-effect transistors [5]. On the contrary, a fast relaxation of hot carriers is beneficial in interband lasers as it populates the lowest states from which light is emitted [1,6]. Also, new technologies are actively searched to harvest hot electrons, [7,8] including hot carrier solar cells which require slowed carrier cooling in the absorber material [9,10]. In this context, playing with quantum confinement appears to be a natural way to tailor the hot carrier dynamics. For example, in strongly confined colloidal quantum dots in which the lowest S and P conduction-band states are separated by several multiples of the optical-phonon energy, there must be a so-called "phonon bottleneck regime" where single phonons cannot cool the carriers any more [11–13].

Beyond these examples, very little is known about the carrier cooling in nanostructures, especially for carriers at high energy where the electronic density of states (DOS) is large and no phonon bottleneck is expected. On the experimental side, carrier cooling has been investigated using pump-probe optical experiments in bulk semiconductors [1] and in nanostructures with various dimensionality [6,13–17] but it remains difficult to extract a detailed picture of the carrier cooling over time and energy.

On the theoretical side, carrier-phonon scattering rates in bulk semiconductors have been calculated using simplified models [1,18], empirical pseudopotentials [19,20], and very recently *ab initio* methods [21–24]. The hot carrier dynamics in small semiconductor nanocrystals has been studied using a surface hopping stochastic simulation method in which the electronic states were obtained with density functional theory [25,26]. The relaxation of hot carriers has also been investigated using various density-matrix formalisms [27–29]. However, the transition from bulk to nanostructures remains to a large extent unexplored as it is very challenging to cover all scales with a common methodology.

In this paper, we present fully atomistic calculations of the carrier cooling in bulk Si and ⟨110⟩-oriented Si nanowires (NWs) using an identical methodology enabling direct comparisons. By varying the NW diameter, we study the transition from small Si NWs to bulk Si. We show that the confinement considerably influences the scattering rates, although the differences with respect to bulk rapidly decrease when the NW diameter increases. At high carrier energy, the carrier cooling is faster in NWs than in bulk. Yet the scattering rates in NWs exhibit steep variations with carrier energy due to the singularities in the electron and phonon DOS resulting from the quantum confinement. As a consequence, there are situations at low carrier energy where the carrier cooling is slower in NWs than in bulk, especially when the carrier has reached the bottom of a conduction-band valley other than ground-state Δ_z valleys.

II. METHODOLOGY

We investigate the relaxation of a single electron (e) or hole (h) initially placed in a high-energy state in the conduction or valence band. We assume undoped materials so that there are no intraband e-e, h-h, and e-h scattering processes, and we do not take impact ionization into account. In this regime of low density of excitation, out-of-equilibrium corrections to the phonon populations are neglected (lattice temperature = 300 K), and therefore the carrier cooling is entirely determined by the carrier-phonon scattering processes that are the main concern of the present work.

The methodology used to calculate the scattering rates is described in our previous works on the modeling of the phonon-limited mobility in bulk Si and Si NWs [30–32]. We use the first-nearest-neighbor tight-binding model of Ref. [33] for the electronic structure, including spin-orbit coupling. On each Si atom, there is a double set of $sp^3d^5s^*$ atomic orbitals, one for each spin orientation. The effects of atomic displacements on the electronic structure are described by bond-length-dependent nearest-neighbor parameters and

*jing.li.phy@gmail.com
†yniquet@cea.fr
‡christophe.delerue@iemn.univ-lille1.fr

strain-dependent on-site terms. In this model, the effects of arbitrary strains on the band energies and effective masses are reproduced in the full Brillouin zone [33]. The NW surfaces are passivated by hydrogen atoms [34].

The phonon states are computed with the valence-force-field model of Ref. [35] which provides a very good description of the bulk phonon-dispersion curves. We do not consider complex reconstructions at the surface, involving for example the formation of dimers. Instead, we passivate all dangling bonds by hydrogen atoms in such a way that all Si bonds are of sp^3 character. In these conditions, we expect that the valence-force-field model can be safely transferred from bulk to NWs.

After diagonalization of the dynamical matrix, we obtain for each wave-vector $\mathbf{q}$ an ensemble of phonon modes j of angular frequency $\omega_j(\mathbf{q})$, characterized by eigenvectors $e^{(j)}(\mathbf{q})$. All modes are considered for the determination of the scattering processes.

The scattering rates are computed with Fermi's "golden rule" for all possible processes where a phonon is either absorbed or emitted. Using a first-order expansion of the tight-binding Hamiltonian ($H = H^{(0)} + H^{(1)} + \cdots$) as a function of the atomic displacements off equilibrium, the transition rate from an electronic state $|\mathbf{k},b\rangle$ in band b, of wave vector $\mathbf{k}$ and energy $E_{\mathbf{k},b}$, to a state $|\mathbf{k}' = \mathbf{k} + \mathbf{q},b'\rangle$ is given by

$$\begin{aligned} &W(|\mathbf{k},b\rangle \rightarrow |\mathbf{k}',b'\rangle) \\ &= \frac{2\pi}{\hbar} \sum_j |\langle H^{(1)}\rangle|^2 \{n(\mathbf{q},j)\delta[E_{\mathbf{k}',b'} - E_{\mathbf{k},b} - \hbar\omega_j(\mathbf{q})] \\ &\quad + [n(\mathbf{q},j)+1]\delta[E_{\mathbf{k}',b'} - E_{\mathbf{k},b} + \hbar\omega_j(\mathbf{q})]\} \end{aligned} \tag{1}$$

where $n(\mathbf{q},j)$ is the equilibrium phonon occupation number (Bose-Einstein distribution). The matrix element of the electron-phonon coupling in Eq. (1) is given by [30]

$$\begin{aligned} \langle H^{(1)}\rangle = &\sum_{\alpha,i} \sqrt{\frac{\hbar}{2NM_\alpha\omega_j(\mathbf{q})}} e^{(j)}_{\alpha i}(\mathbf{q}) \\ &\times \sum_{\beta\eta,\beta'\eta'} C^{\mathbf{k}',b'*}_{\beta'\eta'} C^{\mathbf{k},b}_{\beta\eta} \sum_{m,m'} e^{i\mathbf{k}\cdot\mathbf{R}_{m\beta}} e^{-i\mathbf{k}'\cdot\mathbf{R}_{m'\beta'}} \\ &\times \frac{\partial\langle\phi_{\eta'}(\mathbf{r}-\mathbf{R}_{m'\beta'})|H|\phi_\eta(\mathbf{r}-\mathbf{R}_{m\beta})\rangle}{\partial R_{0\alpha i}} \end{aligned} \tag{2}$$

where β and α denote atoms in the unit cell, and i represents the x, y, and z components of vectors. N is the number of Wigner-Seitz unit cells, and M_α is the mass of atom α. The $C^{\mathbf{k},b}_{\beta\eta}$ are the coefficients of the decomposition of the electronic state $|\mathbf{k},b\rangle$ (solution of $H^{(0)}$ at equilibrium) on Bloch states,

$$|\mathbf{k},b\rangle = \sum_\beta C^{\mathbf{k},b}_{\beta\eta} \sum_m e^{i\mathbf{k}\cdot\mathbf{R}_{m\beta}} |\phi_\eta(\mathbf{r}-\mathbf{R}_{m\beta})\rangle, \tag{3}$$

where $|\phi_\eta(\mathbf{r}-\mathbf{R}_{m\beta})\rangle$ is the atomic orbital η centered on atom β at $\mathbf{R}_{m\beta}$ in the unit cell m.

The final electronic states fulfilling energy and momentum conservation rules are obtained from linear interpolations on a dense mesh in $\mathbf{k}$ space. For bulk Si, we use a mesh of 597 333 $\mathbf{k}$ points, corresponding to 348 6912 tetrahedra. For Si NWs, we use a regular grid of 800 $\mathbf{k}$ points. The carrier cooling is described as a stochastic process with a time step of 0.1 fs. At each step, we calculate the probability [proportional to Eq. (1)] for all possible scattering events. From the knowledge of the total scattering probability, we determine using a stochastic process if the carrier remains in the same state. If it is not the case, a final state is randomly chosen on the basis of the scattering rates.

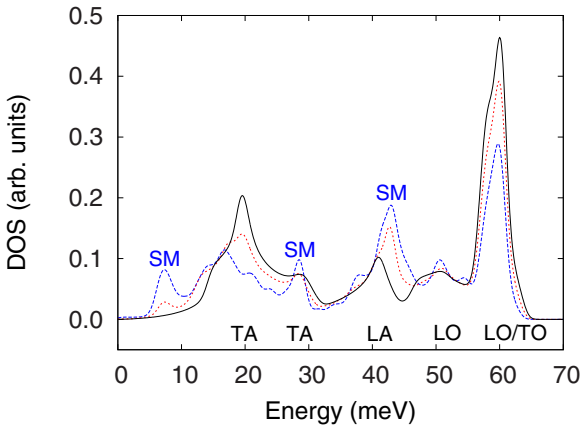

FIG. 1. Phonon DOS per atom in 2-nm NWs (blue dashed line), 5-nm NWs (red dotted line), and bulk Si (black solid line). The main peaks of the bulk DOS are identified for transverse acoustic (TA), longitudinal acoustic (LA), transverse optical (TO), and longitudinal optical (LO) phonon modes. SM denotes surface modes in the DOS for NWs.

III. PHONON DOS

Before discussing the results on the carrier cooling, it is interesting to look at the effects of the confinement on the phonons. The DOS per atom calculated for phonons in Si NWs and bulk Si are presented in Fig. 1. There are important variations between 2-nm NWs and bulk Si, but these differences are already strongly reduced in 5-nm NWs. The peaks in the phonon DOS for bulk Si are also largely present in NWs, allowing us to identify their main origin, transverse or longitudinal, acoustic or optical (Fig. 1). However, it is worth noting that, due to the confinement, phonons in NWs have partially mixed characters. The peaks in the phonon DOS at 8, 28, and 43 meV are specific to NWs. They come from surface phonon modes mostly localized on Si atoms with a Si-Si coordination smaller than in bulk. The DOS for the optical phonons at ∼60 meV is strongly reduced in NWs, the reduction scaling as the surface-to-volume ratio. Part of this DOS is transferred to higher-energy Si-H vibration modes (not shown). The remaining part of the DOS is shifted to lower energy, contributing to the surface modes, especially those at ∼43 meV. Similarly, the DOS at ∼20 meV coming from TA phonons in the bulk is partially transferred in NWs to the surface modes, in the peaks at 8 and 28 meV.

IV. SCATTERING RATES FOR BULK SI

The scattering rates determined as described in Sec. II have been used to calculate the phonon-limited mobility of the carriers in bulk Si. In spite of its semiempirical character, our methodology predicts low-field electron (1407 $\mathrm{cm}^2/\mathrm{V/s}$)

and hole (678 $cm^2/V/s$) mobilities in pretty good agreement with experiment (1400 and 500 $cm^2/V/s$, respectively) [31].

Regarding high-energy excitations, we show in Appendix A that our approach gives total scattering rates for holes in excellent agreement with the *ab initio* data of Ref. [22]. For hot electrons (Appendix B), the agreement is also excellent for excitation energies up to $\sim$1 eV, but our scattering rates exceed the *ab initio* ones for excitation energies between 1 and 2.5 eV. We conclude, nonetheless, that our methodology is essentially validated. The key benefit of the tight-binding approach is that it allows us to investigate carrier cooling not only in bulk Si but also in Si NWs of diameter up to 5 nm.

V. RESULTS FOR SI NANOWIRES

Figures 2(a) and 2(b) display typical time traces of the electron energy in bulk Si and Si NWs. In all cases, the electron is initially placed in a high-energy state ($E = 5$ eV, the zero of energy being the top of the valence band of bulk Si). The discrepancy between the different traces reveals the stochastic character of the carrier cooling. There is no indication of a phonon bottleneck in the figures, despite the formation of well separated subbands in the NWs due to quantum confinement [36,37]. On the contrary, the carrier cooling is faster in thin (2 nm) NWs than in bulk [Fig. 2(a)]. The difference between thicker (5 nm) NWs and bulk is smaller [Fig. 2(b)], but the carrier cooling remains accelerated, and this is particularly visible at the highest energies.

The behavior is basically the same for holes. Figures 3(a) and 3(b) present typical time traces of the hole energy in bulk Si and Si NWs. In all cases, the hole is initially placed in a high-energy state (4 eV from the top of the bulk Si valence band). The decay is faster in 2-nm NWs than in bulk [Fig. 3(a)]. The acceleration is even more obvious than for electrons. The difference is strongly reduced in 5-nm NWs [Fig. 3(b)]. In all cases, the holes have fully relaxed to the valence-band edge of the NW in less than 1 ps. Therefore, the usual belief that the carrier cooling should be slower in nanostructures than in bulk is not founded for high-energy carriers in NWs.

In agreement with these results, Figs. 2(c) and 2(d) show that the electron scattering rates are larger in NWs than in bulk. This is particularly the case for 2 nm NWs while the difference is hardly visible for 5 nm NWs at low excitation energy ($\lesssim$1.5 eV) [Fig. 2(d)]. In this energy range, the rates are, on average, just slightly larger than the bulk values. The scattering rates for holes are also considerably larger in 2 nm NWs than in bulk [Fig. 3(c)]. The difference is strongly reduced in 5-nm NWs [Fig. 3(d)].

A first reason for the enhancement of the scattering rates is the spatial localization of the carrier wave functions: the more localized the carriers, the stronger their coupling to phonons [38]. This explains the general reduction of the low-field carrier mobility in thin NWs [30,31,39,40]. In addition, the selection rules for the conservation of momentum in the transverse direction are partially relaxed in NWs, hence the scattering rates are enhanced further [30,31].

Other effects of confinement are revealed by the nature of the phonons which are either emitted or absorbed during the relaxation. Figure 4(a) shows the distribution of phonons that scatter the electron during the first 0.4 ps. The number

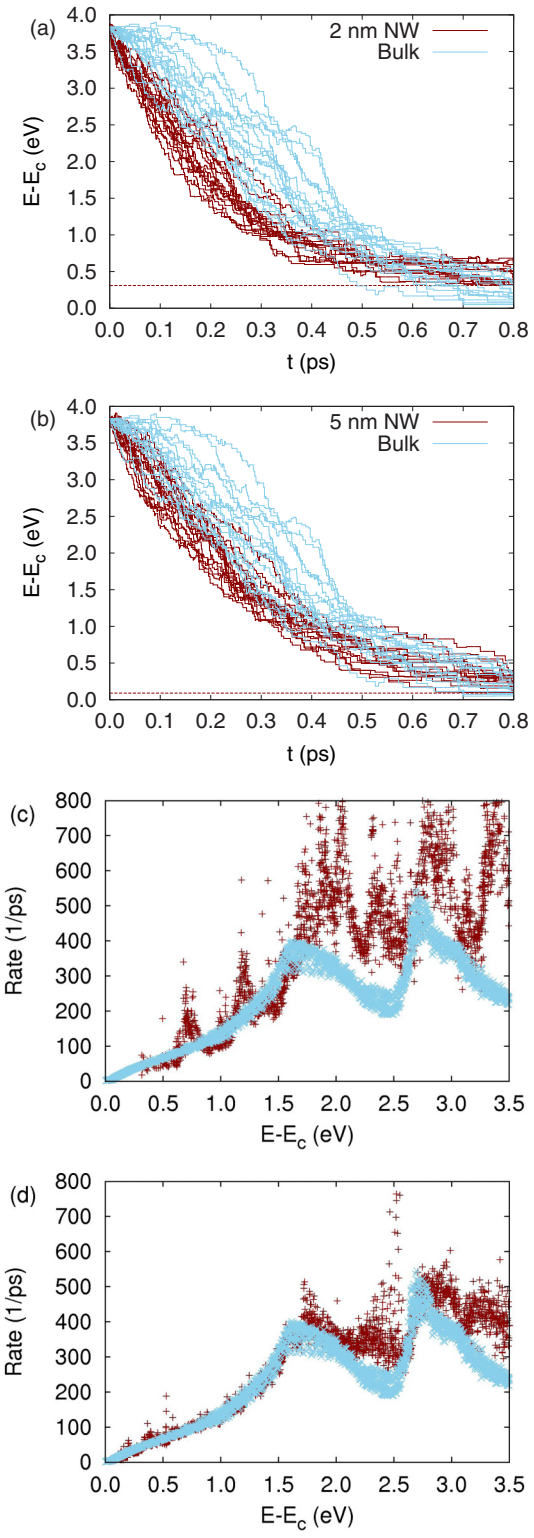

FIG. 2. (a) Energy $E - E_c$ vs time t for an electron initially placed in the conduction band at $E(t = 0) = 5$ eV, the conduction-band edge being at $E_c = 1.17$ eV in bulk Si. Sixteen $E(t)$ traces are shown for bulk Si (sky blue) and for a 2-nm NW (dark red). The dashed horizontal line indicates the conduction-band edge at 1.48 eV for the 2-nm NW. (b) Same as (a), but for a 5-nm NW (conduction-band edge at 1.27 eV). (c) Scattering rate vs electron energy $E - E_c$, in bulk Si (sky blue $\times$) and in a 2-nm NW (dark red $+$). (d) Same as (c), but in a 5-nm NW.

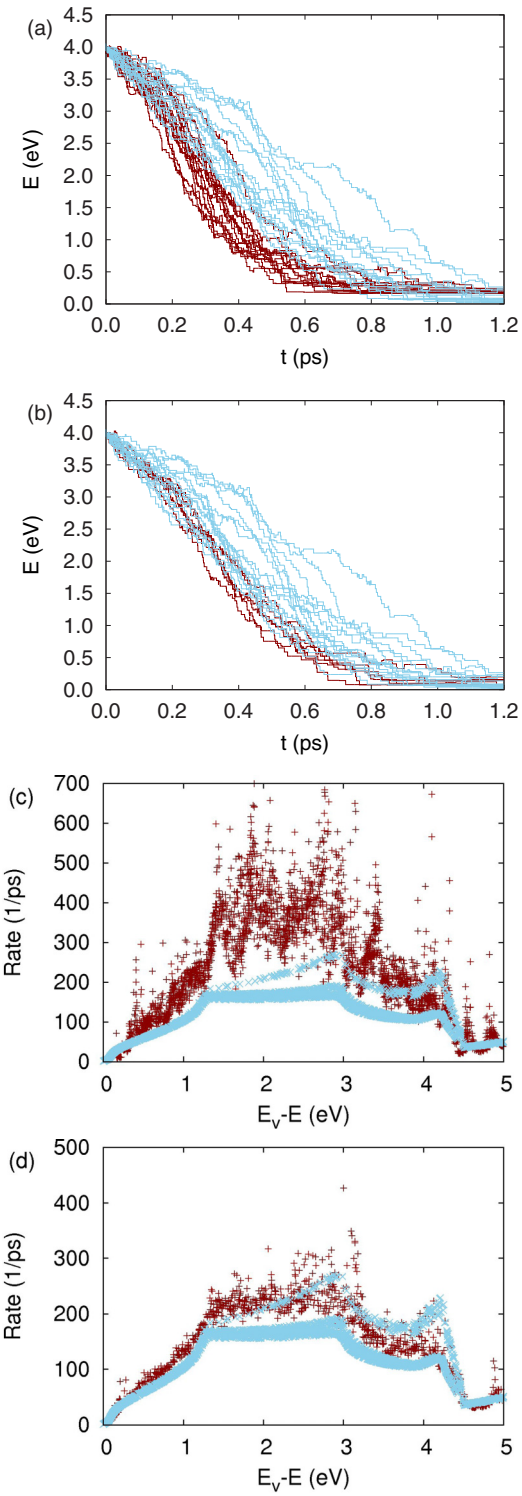

FIG. 3. (a) Energy E vs time t for a hole initially placed in the valence band at $E(t = 0) = 4$ eV, the valence-band edge of bulk Si being at $E_v = 0.0$ eV. Sixteen $E(t)$ traces are shown for bulk Si (sky blue) and for a Si NW with a diameter of 2 nm (dark red). (b) Same for a 5-nm NW. Only six traces are displayed for that NW. (c) Scattering rate vs hole energy $E_v - E$, in bulk Si (sky blue $\times$) and in a 2-nm NW (dark red $+$). (d) Same in a 5-nm NW.

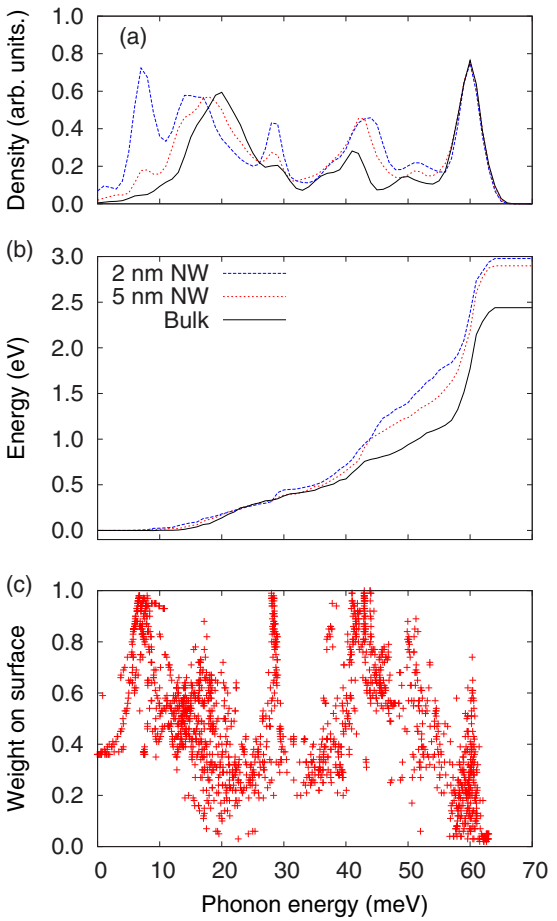

FIG. 4. Analysis of the scattering events occurring during the first 0.4 ps of the 16 $E(t)$ traces shown in Figs. 2(a) and 2(b), for bulk Si (black solid line), a 5-nm NW (red dotted line), and a 2-nm NW (blue dashed line or red crosses). (a) Density of scattering events vs phonon energy $\hbar\omega$. (b) Plot of $R(\hbar\omega)$, the average energy transferred from the hot electron to all phonons of energy smaller than $\hbar\omega$ during the first 0.4 ps. (c) For each scattering event, weight of the normalized phonon eigenvector on Si atoms at the surface of the 2-nm NW.

of scattering events is considerably larger in 2-nm NWs than in bulk, in a wide range of phonon energy. Scattering is still enhanced in a 5-nm NWs, but the distribution of phonons is closer to the bulk reference. The prominent peaks at 8, 28, and 43 meV in Fig. 4(a), also found in the phonon DOS (Fig. 1), are attributed to phonons localized at the surface. This is confirmed by Fig. 4(c) in which we plot, for each scattering event, the weight of the phonon eigenvector on the surface Si atoms as a function of the phonon energy. Surface modes, characterized by a weight close to unity, are strongly involved in the electron cooling in 2-nm NWs. Logically, the intensity of the peaks at 8, 28, and 43 meV in Fig. 4(a) decreases when the NW diameter is increased, the contributions of surfaces becoming progressively less important. Note that Si-H vibrations are not involved in the hot carrier relaxation.

Figure 4(b) shows that only phonons with energy above 30 meV effectively contribute to the carrier cooling because they dissipate more energy and have a much higher probability to be emitted than to be absorbed by the electron at 300 K. In particular, the cooling is much accelerated in NWs by the coupling to surface phonons near 43 meV. This result

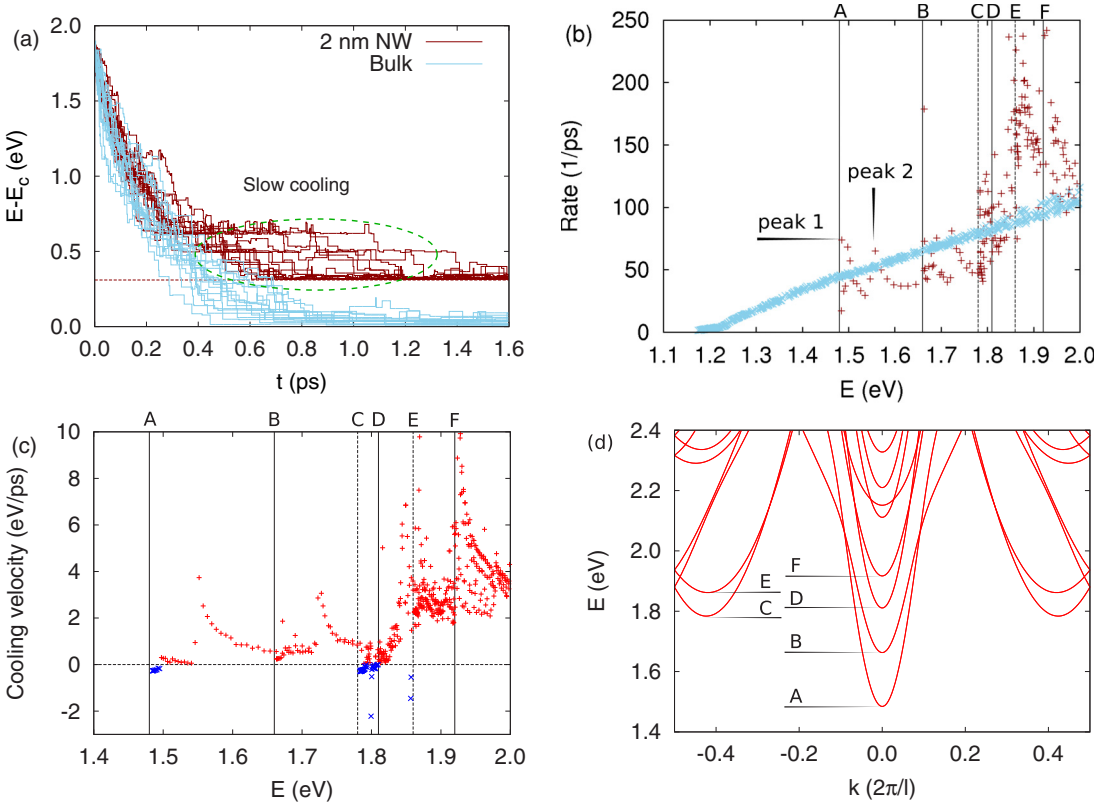

FIG. 5. (a) Energy $E - E_c$ vs time t for an electron initially placed in the conduction band at $E(t = 0) = 3$ eV ($E_c = 1.17$ eV). Sixteen $E(t)$ traces are shown for bulk Si (sky blue $\times$) and for a 2-nm NW (dark red $+$). The dashed horizontal line indicates the conduction-band edge at 1.48 eV for the 2-nm NW. (b) Corresponding scattering rates calculated for all energy states occupied by the electron during the 16 relaxation processes (same color code). (c) Cooling velocity calculated for all conduction-band states in a 2-nm NW (positive values: red $+$; negative ones: blue $\times$). Positive velocities mean that electrons preferentially go to lower energy states. (d) Conduction-band structure of the 2-nm NW. Some subbands are labeled by letters, and the corresponding subband edges are marked by vertical lines in (b) and (c).

confirms the importance of surface effects on the dynamics of hot carriers [6,13,25,26].

The electronic and vibrational structure of NWs is also modified by quantum confinement, with the formation of one-dimensional subbands, for both electrons [Fig. 5(d)] and phonons. The DOS is redistributed and there are peaks at the subband edges (Van Hove singularities). Scattering to the subband edges is therefore enhanced with respect to scattering to the interior of the subbands [Fig. 5(b)]. This explains the sharp variations of the scattering rates with energy, particularly apparent in thin NWs [Figs. 2(c) and 3(c)]. We could imagine that the formation of subbands slows down the carrier cooling because once a carrier has reached the minimum of a subband it must scatter to another subband to release further energy. The large splitting between subbands resulting from strong lateral confinement shall indeed reduce the number of opportunities for intersubband scattering. However, this is hardly visible in a wide range of carrier energies for two reasons. First, there are still many subbands at high energy, which provide adequate final states. Second, the reduction of the number of channels for scattering is overcompensated by the enhancement of the coupling to phonons. We will see in the following that the situation may be different for electrons at low energy, especially in thin NWs, as the conduction-band structure near the gap is considerably modified by the confinement. To demonstrate this, we have considered electrons with initial energy $E = 3$ eV in a 2 nm NW [Fig. 5(a)]. Initially, the cooling rate is comparable to the bulk reference. It takes less than 0.3 ps to drop from 3 to 2 eV. However, in the NW, there are several time traces showing that, in the lowest 0.4-eV energy window, the relaxation can take up to 1 ps. This behavior, not found in the bulk, corresponds to the slow cooling effect usually expected in quantum confined structures.

These results can be understood by looking at the band structure [Fig. 5(d)]. In ⟨110⟩ NWs, the conduction-band minima at $k = 0$ originate from the two Δ_z valleys of bulk Si [36]. The lowest-lying subband A is almost twofold degenerate (fourfold degenerate with spin). The four other $\Delta_{x,y}$ valleys are confined at higher energy and folded at $k \neq 0$. The subbands C and E originate from these valleys. The scattering rates exhibit important variations resulting from the interplay between these different subbands [Fig. 5(b)]. To highlight slow cooling effects, we have plotted another quantity, the cooling velocity, in Fig. 5(c). The cooling velocity of each electronic state is defined as $\sum_i (\pm 1) W_i \hbar\omega_i$, where the sum runs over all possible final states i, W_i is the corresponding scattering rate, and $\hbar\omega_i$ is the energy of the phonon which is either emitted (positive sign) or absorbed (negative sign). The cooling velocity can be extremely small and even negative at the bottom of subbands A and C. In that case, the electron has a higher probability to

be scattered to higher energy via phonon absorption than to lower energy.

The negative cooling velocities at the edge of subbands A are not surprising because the carrier has reached the bottom of the conduction band and cannot be cooled anymore. We have checked that, if we integrate over an increasingly long time, the carrier energy gets distributed according to the equilibrium Fermi-Dirac statistics at 300 K. In Fig. 5(b), peaks 1 and 2 are associated with the fast relaxation of carriers to the edge of subbands A via the emission of acoustic and optical phonons, respectively. As intravalley optical-phonon emission is forbidden in silicon, optical-phonon scattering within subbands A is reminiscent of the g-type ($\Delta_z \rightarrow \Delta_{-z}$) processes in bulk Si [18,41].

The negative cooling velocities at the bottom of subbands C have totally different origins. First, the large DOS brought by the edge of subbands D and E [Fig. 5(d)] promotes phonon absorption. Second, the scattering from subbands C to subbands A, B, D has a comparatively small probability because it is reminiscent of the f-type intervalley processes in bulk Si [18,41]. Therefore the slow cooling evidenced in Fig. 5(a) is due to electrons reaching the bottom of subbands C, and whose relaxation to subbands A, B, D at $k = 0$ can then take about 1 ps. This cannot occur in bulk Si as all valleys have the same energy. There is no significant slow cooling effects anywhere in the valence band of the NWs because the high density of subbands at $k = 0$ accelerates hole-phonon scattering.

The negative velocity predicted for some states just below the edges of subbands E or D can be explained by the high probability of scattering to these subbands characterized by a high DOS (Van Hove singularities).

VI. CONCLUSION AND PERSPECTIVE

In conclusion, we have shown that the confinement may have a profound impact on the carrier relaxation in thin NWs. At low excitation energy where the quantum confinement has the largest influence on the band structure, the cooling can be slowed compared to bulk. This occurs for electrons reaching the bottom of valleys which are not at the conduction-band minimum due to the confinement. On the contrary, the relaxation is accelerated anywhere else at higher energy where the enhancement of the electron-phonon coupling, especially with surface phonons, overcompensates band-structure effects. This shows quite generally that the hot carrier cooling in nanostructures may have a complex behavior that must be further investigated theoretically and experimentally.

The present work must be seen as a first step towards simulations of the hot carrier dynamics in semiconductor nanostructures in all its complexity. At the level of the formalism, it would be interesting to go beyond Fermi's golden rule, for example using a density-matrix formalism in order to understand the effect of the locality on carrier scattering processes [27–29]. Another important issue concerns the incorporation of other scattering mechanisms which may act in parallel with phonon scattering. Even if impact ionization is known to be rather inefficient in bulk Si [42], it would be interesting to compare its relative importance in bulk and nanostructures. More complex problems appear in doped or strongly excited semiconductors. In that case, carrier-carrier interactions play a major role. Indeed, they quickly thermalize the excited carriers so that the effective temperature of the electronic system becomes suddenly much higher than the temperature of the lattice [1]. The complete description of these processes at a microscopic level remains challenging, in particular in nanostructures. Nonetheless, the subsequent cooling of the electronic system takes place by interaction with the phonon bath and therefore the mechanisms described in the present work remain particularly important.

ACKNOWLEDGMENTS

This work was supported by the French National Research Agency (ANR) project "NOODLES" ANR-13-NANO-0009-02.

APPENDIX A: SCATTERING RATES FOR HOLES IN BULK SI

The scattering rates that we have calculated for the holes in the three highest (twofold degenerate) valence bands of bulk Si are plotted in Fig. 6(b). The average rates (defined below) are compared to the *ab initio* calculations of Ref. [22] in Fig. 6(c). The agreement between the two calculations is excellent. For

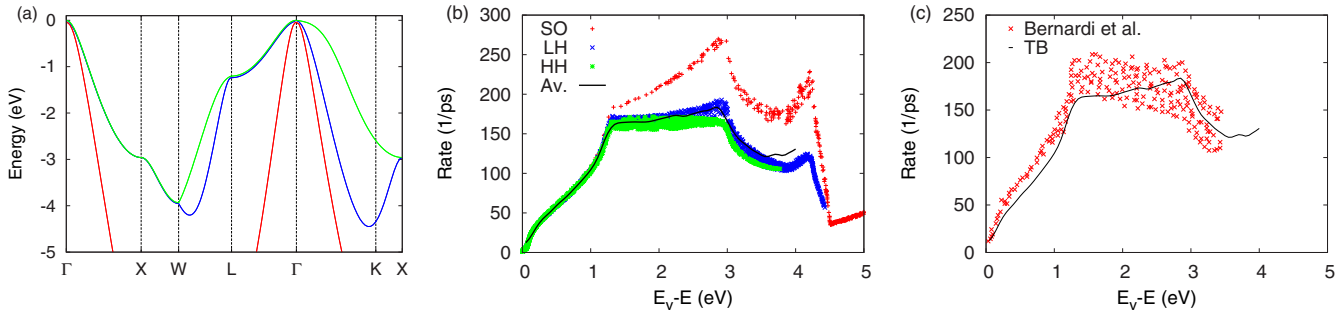

FIG. 6. (a) Valence-band structure of bulk Si calculated in tight binding. The zero of energy corresponds to the top of the valence band ($E_v = 0$). The heavy-hole (HH) band (highest in energy) is plotted in green, the light-hole (LH) band (second in energy) in blue, and the split-off (SO) band (third in energy) in red. (b) Scattering rate vs hole energy $E_v - E$ in the valence band of bulk Si from our tight-binding calculations. The results are presented for initial states in the HH band (green *), the LH band (blue ×), and the SO band (red +). The black solid line represents the scattering rates averaged over the three bands (Av.). (c) The average scattering rates calculated in tight-binding (black solid line) are compared to the *ab initio* calculations of Ref. [22] (red ×).

hole energies ($E_v - E$) above 1.2 eV (corresponding to the heavy- and light-hole band energy at the L point [Fig. 6(a)]), we predict scattering rates slightly larger in the split-off band than in the other valence bands. Above the same threshold, the results of Ref. [22] [Fig. 6(c)] become suddenly very scattered. The origin of the different behavior in the two calculations is not clear at the moment. However, the discrepancies are limited to a small number of points in the $E - \mathbf{k}$ space as the density of states is smaller in the split-off band than in the other bands. The average scattering rate (weighted by the density of states in each band) is actually almost insensitive to the contributions from the split-off band [Fig. 6(c)].

APPENDIX B: SCATTERING RATES FOR ELECTRONS IN BULK SI

Figure 7(b) compares our scattering rates for electrons in bulk Si with those obtained by the *ab initio* calculations of Refs. [21] and [22]. The agreement with the data of Ref. [22] is excellent for energies up to ∼1.7 eV, and with the data of Ref. [21] for energies up to ∼2.2 eV. At higher energies between 2 and 3.5 eV, our scattering rates are larger than the *ab initio* data. Actually, the tight-binding parameters were adjusted to reproduce the band structure of bulk Si at best, but, of course, a stronger emphasis was put on the conduction and valence bands near the gap [33]. This may result in less accurate tight-binding deformation potentials in some energy ranges. Yet we point out that there is a significant spread between the two *ab initio* calculations, although they are both using the local-density approximation to density functional theory. The present tight-binding model reproduces all features of the scattering rates satisfactorily and is applicable to large nanostructures.

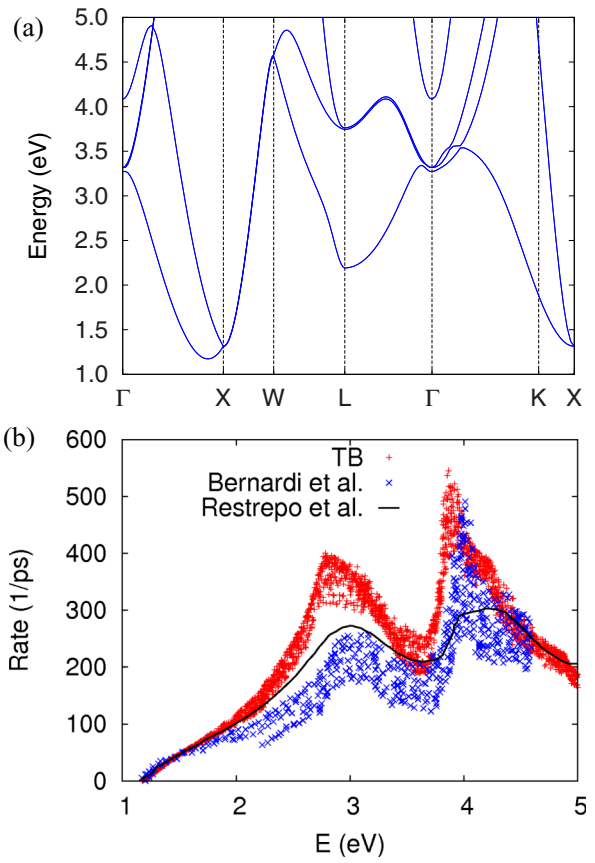

FIG. 7. (a) Conduction-band structure of bulk Si calculated in tight binding. By convention, the zero of energy corresponds to the top of the valence band and the bottom of the conduction band is therefore at $E = E_c = 1.17$ eV. (b) Scattering rate vs electron energy E in the conduction band of bulk Si from our tight-binding calculations (red +) and from the *ab initio* calculations of Ref. [21] (solid line) and Ref. [22] (blue ×).

[1] J. Shah, *Ultrafast Spectroscopy of Semiconductors and Semiconductor Nanostructures*, Springer Series in Solid-State Sciences (Springer, New York, 1999).
[2] W. Shockley and H. J. Queisser, J. Appl. Phys. **32**, 510 (1961).
[3] E. Pop, S. Sinha, and K. E. Goodson, Proc. IEEE **94**, 1587 (2006).
[4] J. Iveland, L. Martinelli, J. Peretti, J. S. Speck, and C. Weisbuch, Phys. Rev. Lett. **110**, 177406 (2013).
[5] C. Guerin, V. Huard, and A. Bravaix, IEEE Trans. Device Mater. Reliab. **7**, 225 (2007).
[6] P. Guyot-Sionnest, B. Wehrenberg, and D. Yu, J. Chem. Phys. **123**, 074709 (2005).
[7] S. Mukherjee, F. Libisch, N. Large, O. Neumann, L. V. Brown, J. Cheng, J. B. Lassiter, E. A. Carter, P. Nordlander, and N. J. Halas, Nano Lett. **13**, 240 (2013).
[8] H. Chalabi and M. L. Brongersma, Nat. Nano **8**, 229 (2013).
[9] R. T. Ross and A. J. Nozik, J. Appl. Phys. **53**, 3813 (1982).
[10] G. Conibeer, N. Ekins-Daukes, J.-F. Guillemoles, D. Knig, E.-C. Cho, C.-W. Jiang, S. Shrestha, and M. Green, Sol. Energy Mater. Sol. Cells **93**, 713 (2009).
[11] U. Bockelmann and G. Bastard, Phys. Rev. B **42**, 8947 (1990).
[12] H. Benisty, C. M. Sotomayor-Torrès, and C. Weisbuch, Phys. Rev. B **44**, 10945 (1991).
[13] A. Pandey and P. Guyot-Sionnest, Science **322**, 929 (2008).
[14] V. I. Klimov, D. W. McBranch, C. A. Leatherdale, and M. G. Bawendi, Phys. Rev. B **60**, 13740 (1999).
[15] Y. Gao, E. Talgorn, M. Aerts, M. T. Trinh, J. M. Schins, A. J. Houtepen, and L. D. A. Siebbeles, Nano Lett. **11**, 5471 (2011).
[16] M. Pelton, S. Ithurria, R. D. Schaller, D. S. Dolzhnikov, and D. V. Talapin, Nano Lett. **12**, 6158 (2012).
[17] D. Tedeschi, M. D. Luca, H. A. Fonseka, Q. Gao, F. Mura, H. H. Tan, S. Rubini, F. Martelli, C. Jagadish, M. Capizzi, and A. Polimeni, Nano Lett. **16**, 3085 (2016).
[18] E. Conwell, in *High Field Transport in Semiconductors*, edited by D. Turnbull and H. Ehrenreich, Solid State Physics Supplements (Academic, New York, 1967).
[19] M. V. Fischetti and S. E. Laux, Phys. Rev. B **38**, 9721 (1988).
[20] T. Kunikiyo, M. Takenaka, Y. Kamakura, M. Yamaji, H. Mizuno, M. Morifuji, K. Taniguchi, and C. Hamaguchi, J. Appl. Phys. **75**, 297 (1994).

[21] O. D. Restrepo, K. Varga, and S. T. Pantelides, Appl. Phys. Lett. **94**, 212103 (2009).
[22] M. Bernardi, D. Vigil-Fowler, J. Lischner, J. B. Neaton, and S. G. Louie, Phys. Rev. Lett. **112**, 257402 (2014).
[23] J. Sjakste, N. Vast, M. Calandra, and F. Mauri, Phys. Rev. B **92**, 054307 (2015).
[24] M. Bernardi, D. Vigil-Fowler, C. S. Ong, J. B. Neaton, and S. G. Louie, Proc. Natl. Acad. Sci. USA **112**, 5291 (2015).
[25] S. Kilina, K. A. Velizhanin, S. Ivanov, O. V. Prezhdo, and S. Tretiak, ACS Nano **6**, 6515 (2012).
[26] K. G. Reeves, A. Schleife, A. A. Correa, and Y. Kanai, Nano Lett. **15**, 6429 (2015).
[27] D. Reiter, M. Glanemann, V. M. Axt, and T. Kuhn, Phys. Rev. B **73**, 125334 (2006).
[28] C. Köhler, T. Watermann, A. Knorr, and E. Malic, Phys. Rev. B **84**, 153407 (2011).
[29] R. Rosati, F. Dolcini, and F. Rossi, Appl. Phys. Lett. **106**, 243101 (2015).
[30] W. Zhang, C. Delerue, Y.-M. Niquet, G. Allan, and E. Wang, Phys. Rev. B **82**, 115319 (2010).
[31] Y.-M. Niquet, C. Delerue, D. Rideau, and B. Videau, IEEE Trans. Electron Devices **59**, 1480 (2012).
[32] Y.-M. Niquet, C. Delerue, and C. Krzeminski, Nano Lett. **12**, 3545 (2012).
[33] Y. M. Niquet, D. Rideau, C. Tavernier, H. Jaouen, and X. Blase, Phys. Rev. B **79**, 245201 (2009).
[34] Y. M. Niquet, C. Delerue, G. Allan, and M. Lannoo, Phys. Rev. B **62**, 5109 (2000).
[35] D. Vanderbilt, S. H. Taole, and S. Narasimhan, Phys. Rev. B **40**, 5657 (1989).
[36] Y. M. Niquet, A. Lherbier, N. H. Quang, M. V. Fernández-Serra, X. Blase, and C. Delerue, Phys. Rev. B **73**, 165319 (2006).
[37] R. Rurali, Rev. Mod. Phys. **82**, 427 (2010).
[38] P. Price, Ann. Phys. **133**, 217 (1981).
[39] M. Luisier, Appl. Phys. Lett. **98**, 032111 (2011).
[40] N. Neophytou and H. Kosina, Phys. Rev. B **84**, 085313 (2011).
[41] C. Jacoboni and L. Reggiani, Rev. Mod. Phys. **55**, 645 (1983).
[42] M. Wolf, R. Brendel, J. H. Werner, and H. J. Queisser, J. Appl. Phys. **83**, 4213 (1998).